THE POTENTIAL INFLUENCE OF RAINFALL ON CALCITE RAFT FORMATION IN GREAT CISTERN SINKHOLE, ABACO ISLAND, THE BAHAMAS

An Undergraduate Research Scholars Thesis

by

KEVIN KELLEY

Submitted to the Undergraduate Research Scholars program at
Texas A&M University
in partial fulfillment of the requirements for the designation as an

UNDERGRADUATE RESEARCH SCHOLAR

Approved by Research Advisor: Dr. Peter van Hengstum

May 2017

Major: Marine Sciences

TABLE OF CONTENTS

ABSTRACT

The Potential Influence Of Rainfall On Calcite Raft Formation In Great Cistern Sinkhole, Abaco Island, The Bahamas

Kevin Kelley
Department of Marine Science
Texas A&M University

Research Advisor: Dr. Peter van Hengstum
Department of Marine Science
Texas A&M University

The stratigraphic record in Great Cistern sinkhole on Abaco Island, The Bahamas, contains coarse-grained layers composed of calcite rafts. Calcite rafts usually form in quiescent cave waters saturated with $CaCO_3$. The appearance of calcite rafts in the Great Cistern sediment record is the first documented occurrence of raft precipitation in a coastal sinkhole. Due to the scarcity of calcite raft formation outside of caves, an examination of raft kinetics, morphology, and ties to regional paleo-environmental factors is warranted. Calcite precipitation in caves can occur at air-water interfaces when the saturation index of water with respect to $CaCO_3$ is near or past equilibrium (i.e., supersaturated), and when there is a higher CO_2 concentration in the water versus the overlying atmosphere. Raft formation at the air-water interface, their external crystal morphology, and longevity are all tied to the kinetic state of the waters from where they derive. Calcite rafts sink below the air-water interface and become part of the local sediment record when the water is agitated, or when the weight of individual calcite rafts (e.g., downward gravitational force) exceeds the force of surface tension buoying them at the surface. It is possible that calcite raft abundance in Great Cistern is a long-term proxy for regional rainfall.

Correlation of calcite raft abundance in Great Cistern sinkhole to $\delta^{18}O$ values from a Cuban speleothem further evaluates the potential of calcite rafts in Great Cistern as a long-term hydroclimate proxy for Abaco.

CHAPTER I

INTRODUCTION

The term ‘calcite rafts’ is the colloquial name given to a very specific morphology of calcium carbonate ($CaCO_3$) crystals that precipitate at an air-water interface. In nature, calcite rafts frequently form in caves on carbonate landscapes, and have only rarely been documented outside of a cave environment. They develop at the surface of quiescent cave waters that are saturated with respect to $CaCO_3$, and with greater CO_2 partial pressures in the water than in the surrounding atmosphere (Taylor & Chafetz, 2004; White 1997). It is thought that calcite rafts can form in less than three months, which gives the rafts time to grow before large amounts of seasonal rainfall destroy them (Taylor & Chafetz, 2004). The raft crystals grow down into the water and can vary in thickness (several microns to 200 microns) (Taylor & Chafetz, 2004; Frisia et al., 2000). The rafts float on the surface tension of the water, and sink due to agitation, or under their own weight due to growth (Taylor & Chafetz, 2004; Frisia et al., 2000). The precipitation of calcite rafts is common in karst cave environments (Palmer, 1991), and rare in non-cave environments. However, calcite rafts have been observed in shallow tufa-lined subaerial pools supplied by ground water (Taylor et al., 2004).

The morphology of calcite rafts is distinctly bipartite: a planar surface characterizes the surface of the mineral in contact with air, and the opposite surface is characterized by euhedral crystal growth. Furthermore, the microcrystalline structure within calcite rafts can be rhombohedral or prismatic (Taylor & Chafetz, 2004). Rhombohedral crystal formation is indicative of slower formation times than prismatic crystal formation, and speed of formation is a

product of the saturation state of the water (Taylor & Chafetz, 2004). Rhombohedral raft crystal structures are termed “fused”, and exhibit formation in very close proximity (Taylor & Chafetz, 2004). Fused structures also have gaps in them indicative of trapped air (Taylor & Chafetz, 2004). Rafts with prismatic morphology termed “interlaced”, tend to form in shorter intervals, and lack the features indicative of trapped gases due to larger distances between individual crystal structures (Taylor & Chafetz, 2004). Crystal morphology is dependent upon saturation state of the solution, whereby ‘fused rafts’ form in waters near equilibrium, and ‘interlaced rafts’ form where saturation states are higher (Taylor & Chafetz, 2004; Teng et al., 2000). The saturation state of groundwater in caves is typically at equilibrium or past equilibrium, whereas the saturation state of seawater is typically near equilibrium (Mucci, 1983). Raft genesis halts when the pCO_2 falls below that of the overlying atmosphere, a change in water ion concentrations, or a large change in turbidation at the site of nucleation (Smart et al., 2006; Taylor & Chafetz, 2004).

In addition, Mucci (1983) demonstrated that the ionization states of the trace minerals in the water also influences the precipitation and dissolution of calcite and aragonite. The stoichiometric solubility constants of calcite increases with salinity because the ionic activity of Ca^{+2} and CO_3^{-2} ions in relation to the increasing ionic strength increases with salinity (Mucci, 1983). An increased solubility constant for $CaCO_3$ means more calcium and carbonate ions can exist in solution without precipitation. This solubility constant increase may in part explain the absence of calcite raft formation in marine or estuarine environments. Calcite rafts can also form in water of varying acidity (pH of 6.70-8.44), but more acidic conditions favor the formation of prismatic raft morphology (Taylor & Chafetz, 2004).

Interestingly, sediment cores collected from a sinkhole on Abaco Island (Great Cistern) contain considerable quantities of coarse grain particles as part of the sedimentary matrix, and these particles are suspected to be calcite rafts. Given the subaerial location of this sinkhole, the presence of calcite rafts is puzzling, and there is no evidence in the literature of calcite rafts having been previously observed in sinkhole sedimentary accumulations. The objectives of this study are to determine the mineralogy, crystal morphology, and depositional timing of these sedimentary particles. These following questions motivate this research:

1. What is the chemistry, mineralogy, and structure of the coarse particles that have accumulated in Great Cistern Sinkhole on Abaco Island?
2. Did coarse particle deposition preferentially occur during specific time intervals? If so, when?
3. What are the potential drivers of coarse particle deposition in Great Cistern Sinkhole on Island through time?

Study Site

The Bahamas are an archipelago of Quaternary carbonate islands in the Western North Atlantic Ocean (Carew & Mylroie, 1997). Of the many islands comprising the Bahamian archipelago, 136,000 km^2 sit atop shallow bank, and 11,400 km^2 is subaerial landmass (Carew & Mylroie, 1997). The shallow banks are usually around 10 m in depth and surrounded by steep drop-offs of great depth (Carew & Mylroie, 1997). Twenty-nine islands, 661 cays, and 2,387 rocks make up The Bahamas, and most of the islands are topographically low-lying (Carew &

Mylroie, 1997). Little Bahama Bank and Great Bahama Bank form are the northwest islands in the Bahamian archipelago, and the banks are separated by the Northwest and Northeast Providence Channels (Carew & Mylroie, 1997). The islands to the southeast are on small banks surrounded by water of varying depths (2000 to 4800 m) (Carew & Mylroie, 1997). Two karst processes dominate the geology of the Bahamas: constructive carbonate deposition and destructive carbonate dissolution triggered by coastal erosion and precipitation (Mylroie et al., 1995). Quaternary glacioeustatic sea-level change have produced observable periods of carbonate deposition as well as denudation (Mylroie et al., 1995). The two major karst landforms of the Bahamas are caves and interior basins (Mylroie et al., 1995). The islands themselves are entirely covered by limestone, and as a result of the porosity of limestone, surface streams are not present on the islands (Mylroie et al., 1995). A meteoric lens of freshwater water is buoyed on saline water below that permeates the islands' limestone bedrock (Mylroie et al., 1995). Flank margin caves are found along coastal areas of the Bahamas and are typically associated with interglacial high stands of sea level (Mylroie et al., 1995). Interior cave systems are typically found at higher elevations (>6 m), and form during glacial and interglacial periods (Mylroie et al., 1995). Most caves on the Bahamas can be traced downward below sea level, and most are largely flooded (Mylroie et al., 1995). The cave systems are often attached to a surface feature termed a sinkhole (Mylroie et al., 1995). There are four types of sinkholes: solution, collapse, suffusion, and subsidence (Kaufmann, 2007; Ford & Williams, 1989). The dominant type of sinkhole found on Great Abaco Island formed through collapse of antecedent carbonate lithology. A collapse sinkhole forms in regions where there is little soil cover over karst rock, and rainwater percolation causes fractures and porosity to form in the rock (Kaufmann, 2007; Ford & Williams, 1989). This secondary porosity eventually enlarges to form caves and

compromises the structural integrity of the rock to eventually cause collapse of overlying material into the subsurface dissolution hole (Kaufmann, 2007; Ford & Williams, 1989). Sinkholes often are connected to a water table and can have extensive subsurface cave formations (Carew & Mylroie, 1997). Coastal sinkholes can become inundated by sea-level rise, and are often times influenced by sea-water percolation via porous karst bedrock (Carew & Mylroie, 1997). Precipitation largely influences karst dissolution and construction patterns in the Bahamas, through the dissolution of karst rock via carbonic acid (Carew & Mylroie, 1997).

In general, the northern Bahamas is characterized by a subtropical temperate climate but there is considerable latitudinal variability in annual rainfall (Carew & Mylroie, 1997). During an annual cycle, there are specific dry and wet seasons, and the wet season on northern islands is interrupted by a decrease in precipitation in July and August formally called the Midsummer Drought (Fig. 1) (Jury et al., 2007; Gamble & Curtis, 2008). On millennial timescales, precipitation in the Caribbean is significantly influenced by meridional displacement of the Intertropical Convergence Zone (ITCZ) and North Atlantic Subtropical High, which is impacted by changing northern hemisphere insolation over Holocene timescales (Hodell et al., 1991; Haug et al., 2001). In general, a more northerly displaced ITCZ increases moisture delivery to the Caribbean, and a more southerly displaced ITCZ increases Caribbean aridity (Fensterer et al., 2013). Environmental proxies (e.g., microfossils, speleothem geochemistry) preserved in sediment records from individual Caribbean Islands can help determine precipitation regime changes due to climate change (Axford et al., 2011; Fensterer et al., 2013).

Great Cistern sinkhole is a coastal sinkhole on Great Abaco Island. Great Abaco Island is the easternmost island mass on the Little Bahama Bank, which is the northernmost carbonate platform in the Bahamian archipelago (Fig. 1). Great Cistern sinkhole has a depth of 9 m and a diameter of 15 m, and it is located less than 40 m from the shoreline at an elevation less than 3 m above mean sea level (msl). The sinkhole is currently flooded by local coastal aquifer, mostly by an upper brackish water lens (surface salinity: 10.8 to 11.3 psu, pH: 7.64). Local tidal impacts can be observed by the daily oscillation of the water level within the sinkhole. The sinkhole is most likely connected into the regional macroporsity of the high porosity and high permeability local aquifer, but diver exploration did not document a cave passage at depth in the sinkhole.

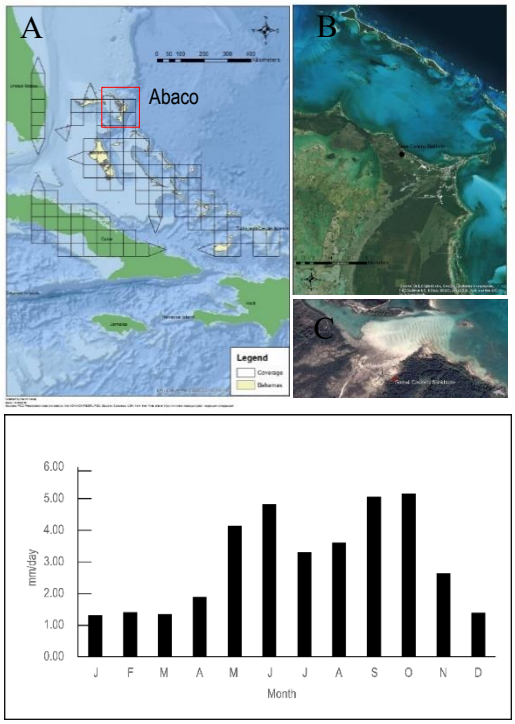

Figure 1. Regional Caribbean average daily precipitation from 1901-2013. A: Regional precipitation study created using weather station data averaged from 1901-2013 grid coverage is 1x1 spatial size and indicates areas of spatial data coverage. B: Satellite imagery of eastern Great Abaco Island, with Great Cistern denoted by a black circle. C: Satellite imagery of Great Cistern sinkhole. Graph: Average daily precipitation data computed from image.

CHAPTER II

METHODS

Regional Precipitation

To understand regional precipitation patterns, two sets of netcdf data files were downloaded, “precip.mon.mean.nc” and “precip.mon.total.v7.nc” from http://www.esrl.noaa.gov/psd/. The files contained precipitation data that was averaged monthly by the Global Precipitation Climatology Centre. The files contained layered monthly precipitation data, the v7 data was taken from weather stations, while the other file was satellite data. The program NCO toolkit was used to obtain a monthly average precipitation for the coverage period for each file. The script used was the following: *ncra –F –d time, 1(indicates month, 1 is January), nmonths (12xnumber of months in file),12 ‘input file name path’ ‘output file name path’*. The script was used twelve times on each separate original netcdf file, with each output name equaling the month that was averaged. The files obtained from the “precip.mon.total.v7.nc” file were imported into ArcMap using the “Make NetCDF Raster Layer” tool. A basic basemap was loaded from the ESRI database for spatial reference. The Caribbean region was zoomed to and each file was exported as a “.tif”, with the coverage set to current. The raster calculator tool was used on each “.tif” file using the formula “file * 1000” to facilitate working with rasters as integers. The 12 new files were named “monthcalc1”, with month indicating the month of the file being analyzed. Raster calculator was used again on the new files utilizing the formula “Int(monthcalc1)”. The new files were labeled “monthint”, with month indicating the month of the file being analyzed. The raster to polygon tool was used on the new files, and the new files were named “monthpoly”, with the same naming convention as the

previous two operations. The attribute table of each file was opened, and a new field was added titled “monthprecip”, with the parameters of the new field being “double” and precision 3. Field calculator was used on the new field using the formula “gridcode/1000” which was done to get the file values back to original values. The union tool was used to join the calculated precipitation files into one table. The table to excel tool was used to export the union file into a Microsoft Excel spreadsheet to produce a bar graph of average monthly precipitation. Each column of precipitation data was averaged in Excel, converted to a column bar graph, and pasted into the ArcMap precipitation map (Fig. 3). The extent of coverage was set to the Bahamas using the v7 precipitation weather station data. The coverage generated from the satellite data was not reproduced due to the small spatial constraints of Abaco Island. The regional precipitation study (Fig. 1) showed an increased period of rainfall from May-October (4-5 mm day^{-1}), with a decrease in precipitation (3.25-3.5 mm day^{-1}) in July and August. The average rainfall for the remaining months ranged from 2-2.5 mm day^{-1}.

Core Collection

In January 2014, a coring survey was conducted in Great Cistern with a Rossfelder P-3 submersible vibracore on a portable raft. An aluminum core pipe was vibrated mechanically until it reached refusal, most likely on antecedent carbonate. Other cores collected from Great Cistern all reached the same depth before refusal on a hard surface that caused damage to the nose (i.e., shoe) of core pipe, which suggests the entire accumulated sediment package from the sinkhole has been sampled. The core examined for the present study was GC-C8, and is 3.54 meters in total length. Cores GC-C7 and GC-C2 were analyzed separately from this study, the results of which were compared to the new results from GC-C8 generated by this work. After collection,

cores were transported back to the laboratory where they were split lengthwise and separated into an archive and a working half for analysis. All data analysis was completed on the working half of the core sections (Fig. 4). Hydrographic conditions in the sinkhole were measured in May 2014 (beginning of wet season) and January 2017 (dry season) with a YSI EXO1 multiparameter water quality sonde, The YSI EXO1 measures salinity (±0.01 psu), dissolved oxygen (±0.1 mg l^{-l}), pH (±0.1), depth (±0.03 m), and temperature (±0.01°C), and was calibrated just prior to field deployment.

Sedimentary Subsurface Texture And Chronology

Sedimentary texture was analyzed in contiguous 1-cm sediment subsamples downcore using the Sieve-first Loss-on-Ignition procedure (*n* = 354 samples) (van Hengstum et al., 2016). The Sieve-first Loss-on-Ignition procedure involved first weighing a set of clean, dry crucibles and recording the masses. A metal sampling spoon was first used to obtain a 2.5 cm^3 sub-samples at 1-cm increments down the length of GC-C8, GC-C7, and GC-C2. The sub-samples were then wet-sieved over a 63-μm mesh, which removed silt- and clay-sized particles (both organic and carbonate). The remaining coarse sediment residue was then carefully washed into an individual crucible and dried overnight in a drying oven. The dried samples were re-weighed, and then subsequently ignited at 550°C for 4.5 hours to remove organic content. The post-burn samples were weighed, recorded, and the values were all entered in a Microsoft Excel spreadsheet. A scatterplot was produced using the coarse fraction amount ($D_{>63\ um}$ mg cm^{-3}) as the dependent variable and total core depth as the independent variable (Fig. 8).

Radiocarbon Dating

Accelerator Mass Spectrometry (AMS) Radiocarbon dating was used to generate a downcore chronology for the sediment core (Fig. 4). Terrestrial plant macrofossils (e.g., leaves, small twigs) weighing >4 mg were sampled from the middle core, and favored over carbonate particles (e.g., gastropod shells) to avoid potential hardwater effects in the radiocarbon signal. Terrestrial plant macrofossils were first rinsed in water, dried overnight at 80°C, and shipped to The National Ocean Sciences Accelerator Mass Spectrometry Facility (NOSAMS) at Woods Hole Oceanographic Institution for radiocarbon measurement. The resultant conventional ages were calibrated into calendar years before present using IntCal13 to account for secular changes in radiocarbon concentration in the atmosphere, where present is 1950 AD (Cal yrs BP_{1950}) (Reimer et al., 2013). A final age-depth model was generated using Bayesian statistical analysis in the R program Bacon v2.2 (Box & Tiao, 2011).

X-Ray Diffraction Analysis

X-Ray Diffraction analysis was used to diagnose the mineralogy of the coarse grained particles that had accumulated in Great Cistern sinkhole. Sediment samples were selected from GC-C8 at the following depths: 134.5, 196.5, 222.5, 272.5, and 355.5 cm. Samples were selected based on abundant coarse fraction content as determined by the Sieve-First LOI procedure. Samples were extracted from the core sections with a metal spatula and sieved using a 63-micron sieve to remove clay and silt particles. The sieved samples were dried overnight in a drying oven at 80°C, and homogenized into a fine powder using a mortar and pestle. The resultant powder was analyzed on a Bruker D8 Advance diffractometer at Texas A&M University in College Station. The sample was placed in the sample holder of a two circle goniometer, enclosed in a radiation safety enclosure. The X-ray source was a 1kW Cu X-ray tube, maintained at an

operating current of 40 kV and 25 mA. The X-ray optics was the standard Bragg-Brentano para-focusing mode with the X-ray diverging from a DS slit (1 mm) at the tube to strike the sample and then converging at a position sensitive X-ray Detector (Lynx-Eye, Bruker-AXS). The two-circle 218 mm diameter θ-θ goniometer was computer controlled with independent stepper motors and optical encoders for the θ circle with the smallest angular step size of 0.0001^{o} 2θ. The software suit for data collection and evaluation is windows based. Data collection was analyzed by employing an automated COMMANDER program employing a DQL file. Data is analyzed by the program EVA. The presence of minerals in the Great Cistern samples were diagnosed by comparing the peaks on the resultant diffractograms with peaks on diffractograms from known standards (e.g., FeOH, $CaCO_3$).

Scanning Electron Microscopy

Photomicrographs of coarse particles from GC-C8 were collected to examine the morphology of mineral particles. Individual sediment particles from GC-C8 were imaged with Hitachi desktop scanning electron microscope (SEM) to determine their external shape and crystal form. First, regions in GC-C8 that had large amounts of potential calcite raft material were identified after the coarse fraction analysis, and based on the presence of calcite from prior x-ray diffractogram analysis. Samples were taken from core depths of 134.5 cm, 162.5 cm, 249.5 cm, and 277.5 cm. The samples were then wet-sieved over a 63-μm sieve, dried overnight at 80°C, mounted on standard aluminum SEM stubs, and gold-sputter coated to increase the electrical conductivity of the samples. Photomicrographs of the sediment particles were saved as raster files (.tiff) for further analysis.

CHAPTER III

RESULTS

Hydrographic Conditions In Great Cistern

Hydrographic conditions for the sinkhole in January 2017 (dry season) (Fig. 3) were brackish throughout the depth of the sinkhole, and a micro-tidal influence was observed from the nearby coast as well. Dissolved oxygen levels in Great Cistern sinkhole were below 1.4 mg/L throughout the water column (Fig. 3). The low dissolved O_2 are indicative of a low energy water environment, and low bioturbation (Strayer et al., 1997). Water temperature was 23°C and pH was 7.3 during January 2017. May 2014 (start of wet season) measurements yielded dissolved oxygen levels of 6-2.4 mg l^{-1} decreasing with water depth, average salinity of 11.3 psu, pH of 7.3, and average water temperature of 25°C.

Sedimentology

Core collection for GC-C8 yielded 360 cm of sediment, and the coring process did not penetrate the antecedent lithology. In general, the top 136 cm of the core was dark-colored organic leaf litter and wood debris (Fig. 2). The organic matter was dark black in color and contained mostly leaf litter and wood pulp, but some sections downcore contained a higher abundance of woody material. The first 136 cm of the core contained very fine sediment (<63 µm) that was easily separated by sieving, which left only organic-rich residue behind on the sieve. Vertebrate bones were also abundant in the core, which were isolated during the sieving procedure. A fish vertebra was found at a depth of 2 cm, possible lizard bones (i.e., anolis) were found at a depth of 255.5 cm, and a total of ten other bones were found (core depths in cm:

256.5, 288.5, 290.5, 291.5, 292.5, 310.5, 313.5, 314.5, and 327.5). Not all bones were easily identifiable, but they are all tentatively identified as belonging to small lizards (i.e., anolis). The last meter of core contained sparse fragments of iridescent insect carapaces (three occurrences), which indicates the excellent sedimentary preservation potential in this basin and limited degradation due to biotic or abiotic factors. Small (<0.5 cm) gastropod shells were sporadically observed downcore, but were not analyzed further. Lastly, the bottom five centimeters of the core was not tested due to a large fragment of wood.

Upon visual inspection of the split core face, there were salient beige-hued horizons downcore with clearly defined contacts. This indicates negligible vertical sediment mixing in the core, or bioturbation. The pale horizons were not evenly spaced, but alternated between organic-rich layers and pale horizons every 2-20 centimeters of core depth. Wood pulp and twigs were present in much of the organic layers, but the color of the organic layers was a lighter brown than the layers shallower in the core before the pale horizons began appearing. Pale horizons varied in size, but were typically 2-10 cm of core length. The two largest hiatuses of pale horizon occurrence appeared between depths of 160.5 cm to 173.5 cm and 305.5 cm to 311.5 cm.

The Sieve-First LOI procedure was used to identify downcore changes in coarse mineral particles, and these beige-hued horizons consistently contained coarser particles relative to the dark-hued organic-rich intervals. The quantity of coarse sediment particles began gradually increasing at 146.5 cm (Fig. 2). Coarse particle abundance ranged from 5-20 mg cm^{-3} from the top of the core to a depth of ~144.5 cm. Significant increase in coarse abundance occurred at the following depth intervals: 144.5-158.5 cm, 176.5-184.5 cm, 187.5-204.5 cm, 219.5-232.5 cm,

242.5-307.5 cm, 310.5-351.5 cm. The corresponding coarse grain sizes were as follows: 27.5-85 mg cm^{-3}, 194-200 mg cm^{-3}, 131-308 mg cm^{-3}, 101-170 mg cm^{-3}, 113-390 mg cm^{-3}, 100-356 mg cm^{-3}. Overall, the texture of these beige horizons increased downcore. Coarse particle sizes measured in dark-hued horizons increased with core depth, and measure 100 mg cm^{-3} or less throughout the core until 311.5 cm core depth. From 311.5 cm to the core bottom there were less distinct pale and dark-hued horizons, which was likely due to the high number of $CaCO_3$ particles. Coarse particle size ranges for the dark-hued regions ranged from 5-200 mg cm^{-3}; however, the darker-hued regions containing near 200 mg cm^{-3} particle sizes had visibly lighter hues than dark-hued horizons with less than 100 mg cm^{-3} particle sizes.

X-Ray Diffraction (Fig. 5) confirmed the mineralogy of the coarse particles in GC-C8 as calcite. The coarse particle horizons resembled $CaCO_3$ sand superficially, but showed resemblance to calcite raft material under optical microscopy. Further analysis of particle morphology under scanning electron microscopy revealed rhombohedral, fused rafts that made up the coarse particle horizons within each sediment core (Fig. 4). Dissolution marks are also visible, as well as small holes indicative of trapped gases (Taylor & Chafetz, 2004).

Chronology

Radiocarbon dating of terrestrial plant macrofossils from GC-C8 indicated that all sediment accumulated during the middle to late Holocene. Samples for radiocarbon dating (leaf litter), were taken at 98, 128, 226, 251, and 303 cm core depths and had corresponding ages 1260 ± 15, 1740 ± 15, 2770 ± 20, 3120 ± 20, and 4460 ± 25 Calibrated years before present (Cal yrs BP, Fig. 2). A final age model for the core was generated with the R program *Bacon*, which uses

a Bayesian statistical approach to develop a relationship downcore between the depth of the core and age (Fig.6).

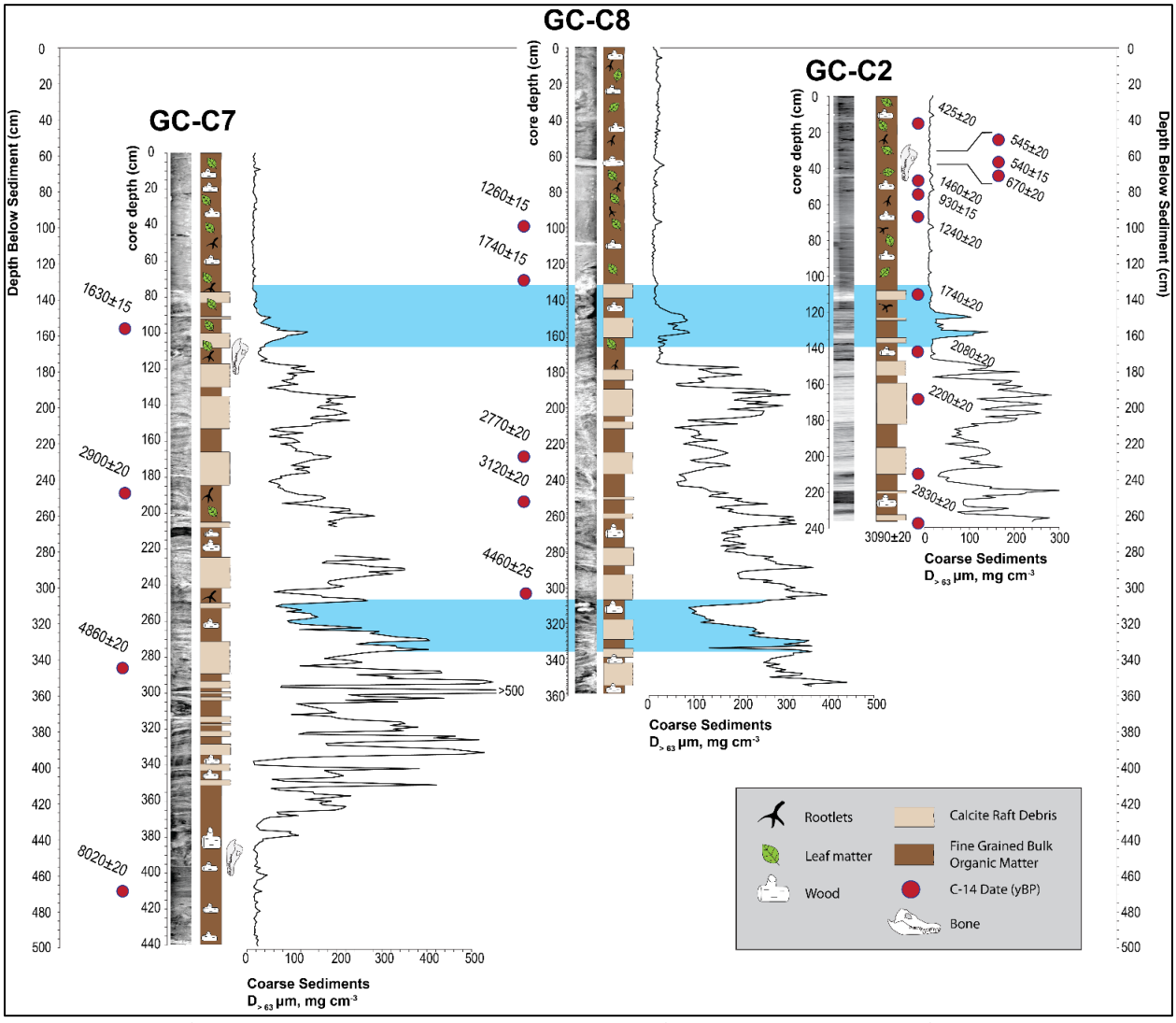

Figure 2. Core logs. Left-Right: GC-C7, GC-C8, and GC-C2 matched with coarse fraction peaks denoting calcite raft material. X-Radiographs matched to the core logs have lighter shading to denote denser sediment layers. Top blue shaded region shows cessation of coarse particle occurrence in all three cores, and bottom blue region shows another hiatus of raft deposition. GC-C7 and GC-C2 were processed separately.

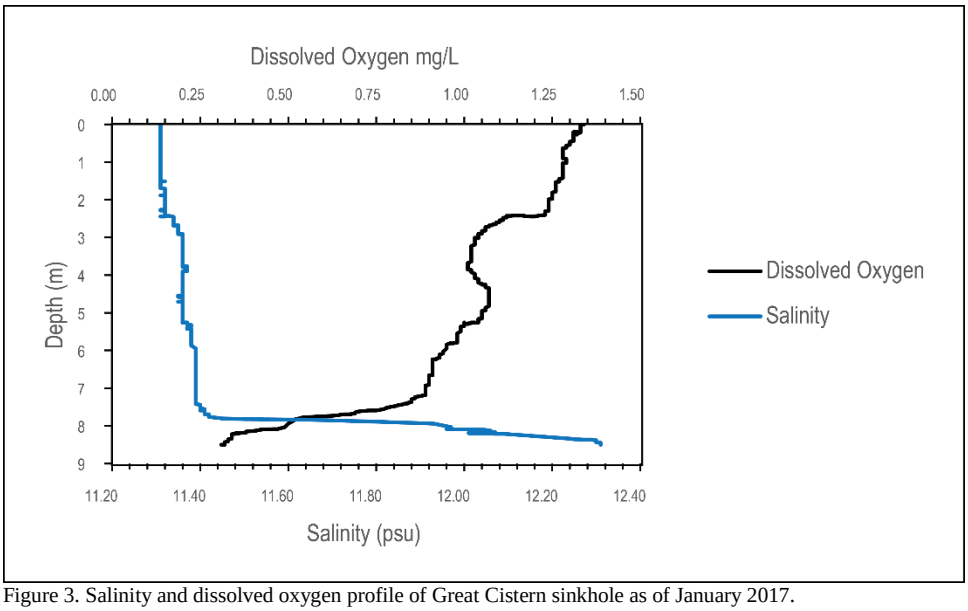

Figure 3. Salinity and dissolved oxygen profile of Great Cistern sinkhole as of January 2017.

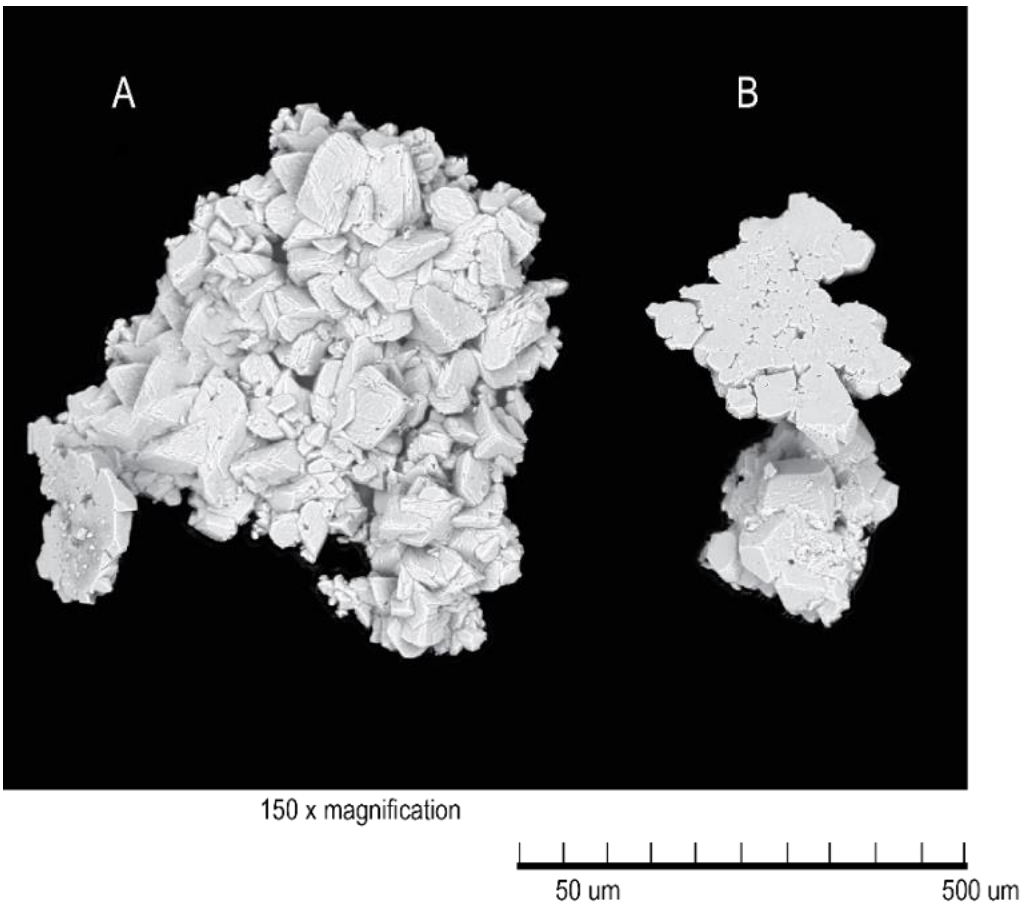

Figure 4. Calcite raft material from Great Cistern sinkhole. A: Planar (growth) side up. B: Surface of raft material where air/water interface was located. Dissolution marks are present as well as spaces where trapped gases were present.

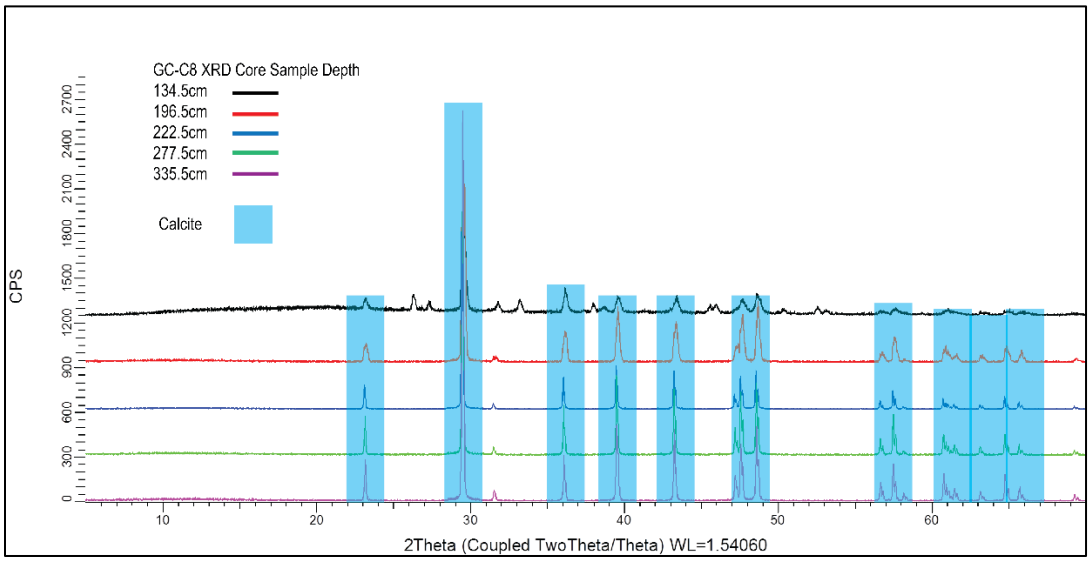

Figure 5. X-Ray diffractograms with highlighted peaks indicating the presence of calcite.

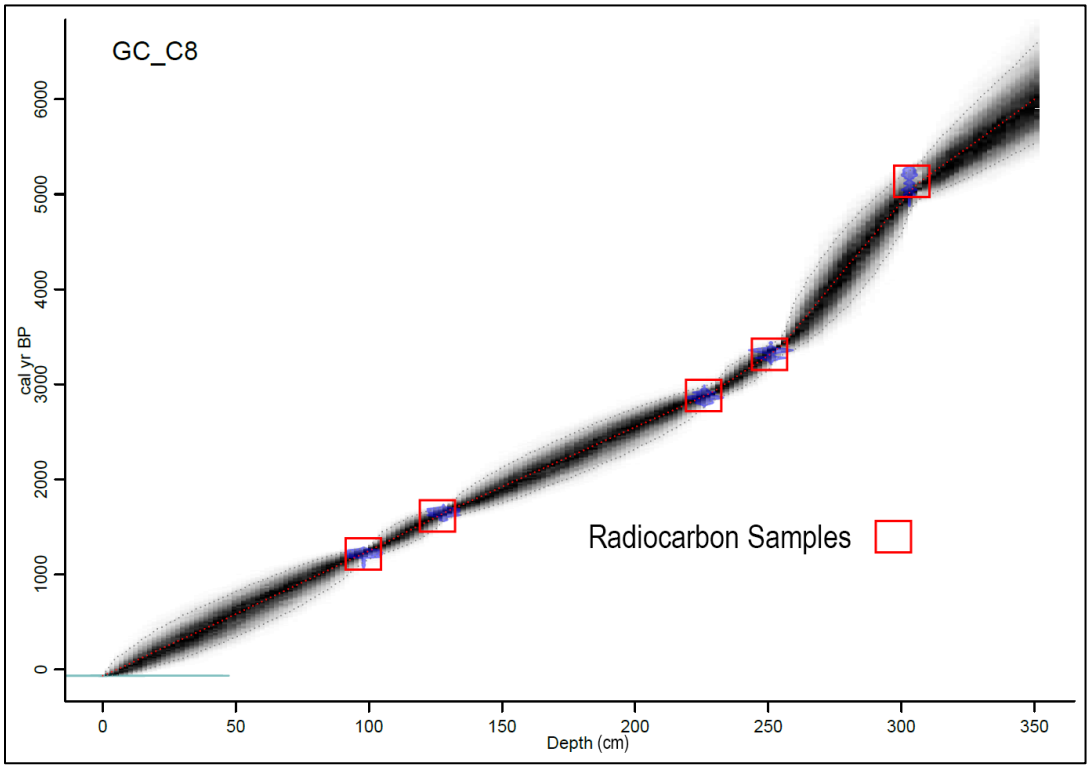

Figure 6. Age plot versus core depth created using Bayesian statistical analysis in the R program Bacon v2.2 (Box & Tiao, 1992).

CHAPTER IV

DISCUSSION

Sedimentation Patterns In Great Cistern Sinkhole

GC-C7 and GC-C2 were taken within several meters of GC-C8 and analyzed separately in another study. GC-C8, GC-C7, and GC-C2 all exhibit an increase in the occurrence of coarse particle (sand) deposition as beige horizons between ~1600 to 7200 Cal yrs BP. After further analysis (see Figs. 4, 5), the coarse particles were diagnosed as calcite rafts. The beige horizons became more pronounced where each core was dated near 1.6 Cal yrs BP. The close correlation of pale sediment horizons between the three cores confirms contiguous stratigraphy in the basin. Of the three cores, GC-C7 is the only core believed to have penetrated the complete sedimentary package in the basin, while GC-C8 and GC-C2 do not contain the entire Holocene sequence in the basin. Due to the incomplete sediment packages of GC-C2 and GC-C8, the core logs had to be matched based on coarse particle size, and radiocarbon dated age markers. Once the radiocarbon markers were matched, coarse particle peaks all showed the same general trends downcore. GC-C7 contained more bones than GC-C2 and GC-C8, but the bone types (terrestrial anolis lizards downcore, fish bones upcore), remained consistent in each core. Dark-hued organic layers were present in each core, and comprised the entirety of each cores sedimentology prior to the appearance of pale horizons at 1600 Cal ys BP. The dark-hued organic layers did not disappear at the onset of the pale layers, but continued to occur between the pale layers. The continued appearance of dark organics between the pale horizon layers suggests the supply of organic material to Great Cistern did not interfere with precipitation of the pale horizon calcite particles. The color of the dark-hued horizons lightened with depth in each core from a near

black (prior to the pale horizons), to light brown (near 300-500 mg cm^{-3}coarse particle size). The color change shows a trend of maximum calcite particle precipitation downcore, and a lack of calcite precipitation upcore prior to ~1600 Cal ys BP. Pale coarse particle layers disappeared from the sediments in GC-C7 at 350 cm core depth, while GC-C8 and GC-C2 showed evidence of calcite rafts throughout the later sections of the core to the bottom. Pale horizons varied in length from a few centimeters to several, indicating sedimentation of the coarse particles occurred in long intervals (years), and not at equal rates. There are two notable decreases pale horizon occurrence in all three sediment cores (Fig.2) that coincide with radiocarbon dates of ~1700 Cal ys BP and ~4400 Cal yrs BP. The pale horizon particles are calcite and have episodic depositional characteristics captured in three sediment cores.

Drivers Of Calcite Precipitation

The precipitation of calcium carbonate occurs based on the chemical equation:

$$Ca^{2+} + 2HCO_3^- \leftrightarrow CaCO_{3(solid)} + CO_2 + H_2O$$

Precipitation of calcite in freshwater depends on multiple factors. For calcite precipitation to occur, the pCO_2 of the water must be higher than the surrounding atmosphere (Mucci, 1983). If calcite concentrations in the water are near equilibrium, the water surface will interact with the atmosphere (with or without turbulence), which causes off-gassing of CO_2 from the water (Mucci, 1983). The off-gassing of CO_2 leads to an increase in pH of the water, and a subsequent further saturation state with respect to calcite (Mucci, 1983). Alkaline waters favor calcite precipitation, and increased temperature can lead to increased evaporation, which subsequently leads to increased calcite saturation (Mucci, 1983). Calcium carbonate precipitation in seawater seems plausible upon calculation (Eq. 1, 2, and 3). Determining the degree of saturation with

respect to $CaCO_3$ in seawater at 35 psu yields a degree of saturation of 630, with values less than one indicating undersaturation and values over one as supersaturated. Values were taken from the 97th CRC Handbook of Chemistry and Physics (Haynes, 2016).

Solubility product constant (saturated conditions): (Eq. 1)

$$K_{sp} = [M^{+}_{Ca\ ion}][A^{-}_{calcium\ carbonate\ ion}] = 3.35\ \times\ 10^{-9}$$

Ion Product $CaCO_3$: (Eq. 2) Concentrations obtained from the CRC handbook (Haynes, 2016).

$$IP =\ [Ca^{2+}][CO_3^{2-}] = 2100 \times 10^{-9}$$

Degree of saturation: (Eq. 3)

$$\Omega = \frac{Ion\ Product}{K_{sp}} =\ \frac{2100\ \times\ 10^{-9}}{3.35\ \times\ 10^{-10}} = 630$$

Degree of saturation should promote precipitation of calcite from seawater, yet calcite does not readily precipitate due to ionic activity interference likely caused by the other salts in seawater (Mucci, 1983; Plummer, 1975). The reason calcite does not precipitate in seawater is not fully understood, but salinity likely plays a large role. Plummer (1975) stated that interactions between saturated fresh and saltwater at meteoric lens' in the Bahamas yields a product that is undersaturated, which he attributes to ionic interference of the seawater (1975). Dissolution of limestone has been observed through the interaction of the groundwater meteoric lens under The Bahamas (Plummer, 1975). The dissolution of caves in carbonate systems has also been attributed to the erosive effects of marine water interaction with freshwater lenses (Mylroie & Carew, 1990). If dissolution of limestone ($CaCO_3$) lithology is common in karst environments in The Bahamas, then it is plausible that saltwater intrusion into Great Cistern

1600 Cal yrs BP halted calcite raft precipitation. The reason salinity affects inorganic calcite precipitation is a matter of debate. Mucci calculated that solubility product constants rise exponentially with salinity increase (Fig. 9), which would potentially allow calcite to exist in solution in high concentrations without precipitation (1983; Plummer, 1975). The environment on Abaco Island, The Bahamas was different from present day. Sea level curves suggest the sinkhole has not been inundated by the sea during the last 7000 years, but the porous limestone that The Bahamas sits on allows seawater intrusion into the island from below (Ford & Williams, 1989; Milne & Peros, 2013; Mylroie & Carew, 1990). Sea level was ~12 m lower relative to present ~7800 Cal yrs BP (Milne & Peros, 2013). This would have caused a water depth of roughly 1 m in Great Cistern sinkhole (Milne & Peros, 2013). The lower sea level would have meant little to no sea interaction with the sinkhole, which would have promoted near limnic conditions in the sinkhole. The shallow water depth of the sinkhole, and lack of tidal disturbance within the sinkhole, would make for a quiescent environment suitable for calcite raft genesis, despite the hole being open to the atmosphere (Taylor et al., 2004). Sea level was 1 m lower along the Bahama Banks 100 years ago than it is currently (Milne & Peros, 2013). Sea level intrusion into the karst bedrock surrounding the sinkhole would have also introduced additional salts found in seawater to the previously fresh sinkhole water. The increased salinity, and thus increased ionic interference, would have raised the solubility product constants for calcite, and increased the activity coefficients in the sinkhole water (Mucci, 1983; Mylroie & Carew, 1990). Lower pCO_2 in the water versus the overlying atmosphere of the sinkhole could have halted raft genesis, but there is not any reason for this to occur since groundwater is typically saturated with CO_2 (Palmer, 1991;White, 1997). The sinkhole was likely fed by an underground fresh aquifer, which would have been saturated with respect to $CaCO_3$ (Kaufmann, 2007). Increased periods of

rainfall would allow water to percolate through the limestone bedrock, pick up additional Ca^{+} ions, and enter the sinkhole (Ceron et al., 2002; Kaufmann, 2007). In summary, there are multiple factors that theoretically control calcite raft formation, but the most likely reason for a ceasation in their formation in the last ~1600 years is likely due to an increase in slainity in the sinkhole, which generated unfavourable conditions for raft nucleation and growth.

Potential Linkage Of Calcite Raft Sedimentation To Long-Term Bahamian Precipitation

The abundance of calcite rafts in Great Cistern sediment record are potentially providing evidence for prehistoric precipitation activity on Great Abaco Island, given their accumulation patterns mimic known long-term trends of regional precipitation. The period from 8200 to 2500 Cal yrs BP was a period of increased solar insolation due to Earth's orbital precession, which caused a climate shift from arid to mesic on Haiti (Hodell, et al., 1991). In the Bahamas, periods of heavy rainfall would have introduced $CaCO_3$ ions into Great Cistern sinkhole, which would have raised the saturation state of the water in the sinkhole. The calcite rafts would have been able to precipitate in an environment chemically similar to a cave (the usual place calcite rafts appear) (Taylor et al., 2004). During periods of decreased rainfall, the saturation state of the water would drop below equilibrium and make calcite precipitation unfavorable. In addition, the accumulation of calcite rafts in the sinkhole are closely correlated with stable oxygen isotopic ratios ($\delta^{18}O$) archived in a Cuban speleothem, which determined periods of increased versus decreased rainfall in Cuba (Fig. 7)(Fensterer et al., 2013). Low $\delta^{18}O$ values (more negative) indicate wetter conditions, higher $\delta^{18}O$ values (more positive) indicates drier conditions (Fensterer et al., 2013). The correlation shows that the intervals with more negative $\delta^{18}O$ values in the speleothem are coeval with increased calcite raft deposition in Great Cistern sinkhole. The correlation between raft deposition and periods of increased precipitation determined by

Fensterer et al. (2013) would suggest that the calcite rafts within the sediment record of Great Cistern sinkhole can serve as a proxy for rainfall on Great Abaco Island. Calcite raft occurrence indicates waters near or past equilibrium, and gives a general idea of calcium ion saturation index, pCO_2, pH, temperature, as well as general energy environment within the sinkhole (Mucci, 1983; Taylor & Chafetz, 2004; Teng et al., 2000; White, 1997). Fensterer et al. (2013) documented general pattern of increasing precipitation through the middle Holocene in the Caribbean . ~4500 years ago, however, both the Cuban speleothem and calcite raft deposition decrease, and likely indicate a period of regional drought (Fig. 8). From 3300 to 2500 Cal yrs BP, the Cuban speleothem ceased growing (Fensterer et al., 2013), which is timed with decreased accumulation of calcite rafts in Great Cistern Sinkhole. The latitudinal variability of Caribbean precipitation, combined with other physical factors that could control speolethem development, could have caused the difference in precipitation records (Ford & Williams, 1989). Further examination of additonal Caribbean hydroclimate proxies is required to solidfy a clearer paleoclimate picture for the time period of raft deposition. The calcite rafts do offer a valid hydrological piece of evidence for an overall hydroclimate reconstruction of the region.

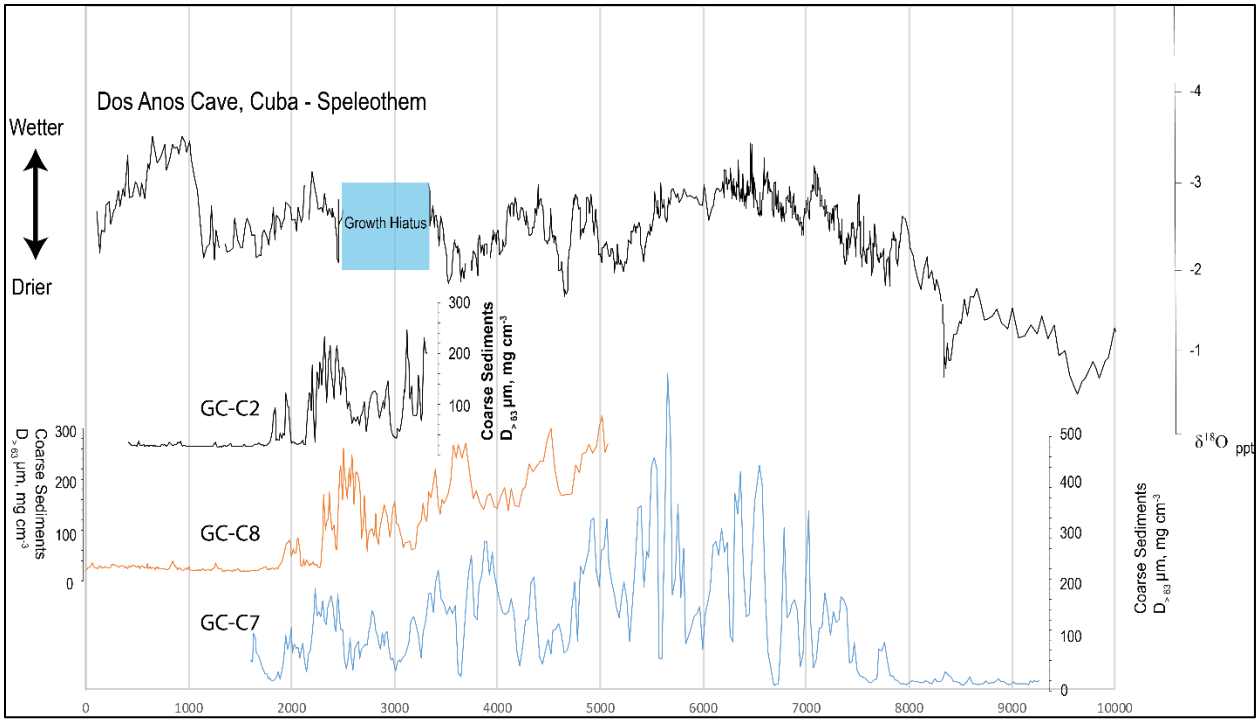

Figure 7. Coarse sediment amount peaks compared to Fensterer et al., (2013) Dos Anos Cave, Cuba speleothem $\delta^{18}O$ (‰ VPDB) values showing correct wet and dry peak correlations.

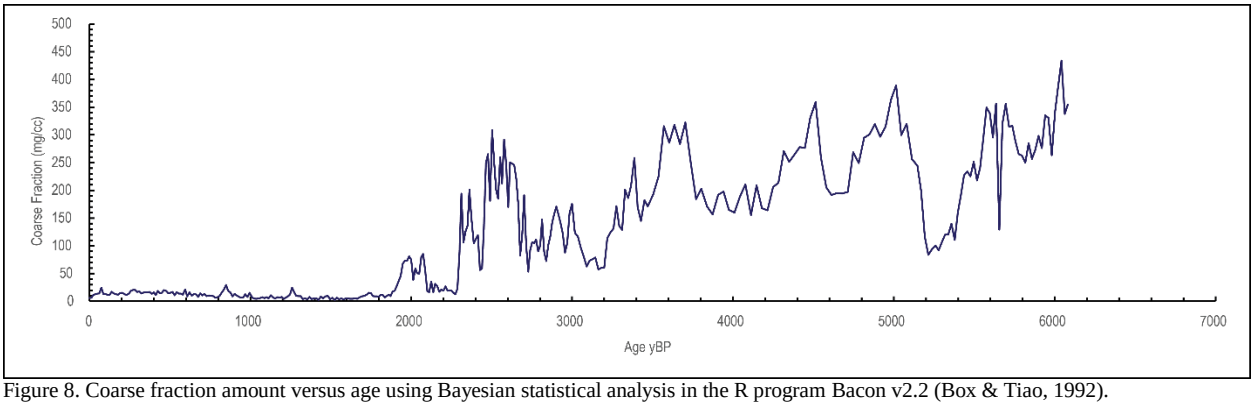

Figure 8. Coarse fraction amount versus age using Bayesian statistical analysis in the R program Bacon v2.2 (Box & Tiao, 1992).

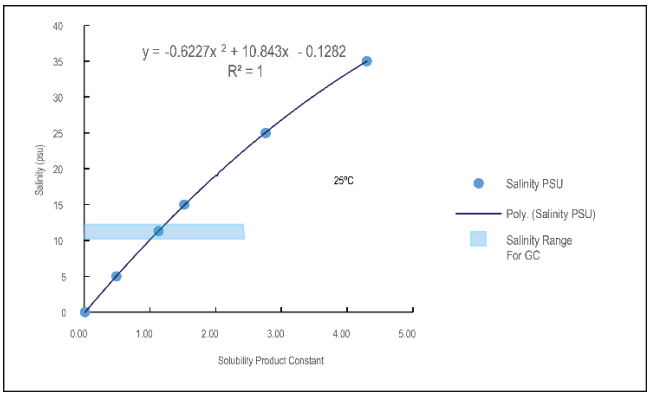

Figure 9. Solubility product constants at 25ºC and various salinities. Taken from experimental values produced by (Mucci, 1983).

CHAPTER V

CONCLUSION

The sediment record from Great Cistern sinkhole on Abaco Island, The Bahamas, contains abundant pale-beige horizons that were diagnosed as being horizons of calcite rafts. Deposition of these calcite rafts occurred from 7200 to 1600 Cal yrs BP, but the abundance of calcite raft accumulation changed through time. Calcite raft deposition, both long-term and centennial-scale oscillations, correlates with changes in stable oxygen isotopic ratios preserved in a Cuban speleothem. This means the rafts are a paleohydrological proxy for Abaco Island, and potentially the entire northern Caribbean region. The disappearance of the rafts ~1600 years ago was likely tied to the increased salinity in the sinkhole from saltwater intrusion from changing coastal geometry related to Holocene relative sea-level rise (e.g., shoreline translation, coastal embayment). These results demonstrate that calcite rafts in Great cistern may serve as useful proxy of regional precipitation patterns.

REFERENCES

Axford, Y., Andresen, C. S., Andrews, J. T., Belt, S. T., Geirsdottir, A., Masse, G., . . . Vare, L. L. (2011). Do paleoclimate proxies agree? A test comparing 19 late Holocene climate and sea-ice reconstructions from Icelandic marine and lake sediments. *Journal of Quaternary Science 26(6)*, 645-656.

Box, G. E., & Tiao, G. C. (2011). *Bayesian inference in statistical analysis* (Vol. 40). John Wiley & Sons.

Carew, J. L., & Mylroie, J. E. (1997). *Geology and Hydrogeology of Carbonate Islands.* . Elsevier .

Ceron, R., Padilla, H., Belmont, R., Torres, M., Garcia, R., & Baez, A. (2002). Rainwater chemical composition at the end of the mid-summer drought in the Caribbean shore of the Yucatan Peninsula. *Atmospheric Environment (36)*, 2367-2374.

Fensterer, C., Scholz, D., Hoffmann, D. L., Spotl, C., Schroder-Ritzrau, A., Horn, C., . . . Mangini, A. (2013). Millennial-scale climate variability during the last 12.5 ka recorded in a Caribbean speleothem. *Earth and Planetary Science Letters 361*, 143-151.

Ford, D., & Williams, P. (1989). *Karst Geomorphology and Hydrology.* London: Unwin Hyman Ltd.

Frisia, S., Borsato, A., Fairchild, I. J., & McDermott, F. (2000). Calcite Fabrics, Growth Mechanisms, and Environments of Formation in Speleothems From the Italian Alps and Southwestern Ireland. *Journal of Sedimentary Research 70*, 1183-1196.

Gamble, D. W., & Curtis, S. (2008). Caribbean precipitation: review, model and prospect. *Progress in Physical Geography 32 (3)*, 265-276.

Haynes, W.M. (2016). *CRC Handbook of Chemistry and Physics,* 97th Edition. CRC Press.

Haug, G.H., Hughen, K.A., Sigman, D.M., Peterson, L.C., Rohl, U., 2001. Southward migration of the intertropical convergence zone through the Holocene. *Science 293, 1304-1308.*

Hodell, D. A., Curtis, J. H., Jones, G. A., Higuera-Gundy, A., Brenner, M., Binford, M. W., & Dorsey, K. T. (1991). Reconstruction of Caribbean climate change over the past 10,500 years. *Nature (vol. 352)*, 790-792.

Jury, M., Malmgren, B. A., & Winter, A. (2007). Subregional precipitation climate of the Caribbean and relationships with ENSO and NAO. *Journal of Geophysical Research 112*.

Kaufmann, J. E. (2007). Sinkholes. *USGS Fact Sheet*, 3060.

Milne, G. A., & Peros, M. (2013). Data-model comparison of Holocene sea-level change in the circum-Caribbean region. *Global and Planetary Change (107)*, 119-131.

Mucci, A. (1983). The solubility of calcite and aragonite in seawater at various salinities, temperatures, and one atmosphere total pressure. *American Journal of Science (Vol. 283)*, 780-799.

Mylroie, J. E., & Carew, J. L. (1990). The Flank Margin Model for Dissolution Cave Development in Carbonate Platforms. *Earth Surface Processes and Landforms 15*, 413-424.

Mylroie, J. E., Carew, J. L., & Vacher, H. L. (1995). Karst development in the Bahamas and Bermuda. *Special Papers - Geological Society of America* , 251-268.

Palmer, A. N. (1991). Origin and morphology of limestone caves. *Geological Society of America Bulletin 103*.

Plummer, L. N. (1975). Mixing of sea water with calcium carbonate ground water. *Geological Society of America Memoirs, 142*, 219-236.

Reimer, P. J., Bard, E., Bayliss, A., Beck, J. W., Blackwell, P. G., Ramsey, C. B., ... & Grootes, P. M. (2013). IntCal13 and Marine13 radiocarbon age calibration curves 0–50,000 years cal BP. *Radiocarbon*, *55*(4), 1869-1887.

Schneider, Udo; Becker, Andreas; Finger, Peter; Meyer-Christoffer, Anja; Rudolf, Bruno; Ziese, Markus (2011): GPCC Full Data Reanalysis Version 6.0 at 0.5°: Monthly Land-Surface Precipitation from Rain-Gauges built on GTS-based and Historic Data. DOI: 10.5676/DWD_GPCC/FD_M_V7_050

Smart, P. L., Beddows, P. A., Coke, J., Doerr, S., Samantha, S., & Whitaker, F. A. (2006). Cave Development on the Caribbean coast of the Yucatan Peninsula, Quintana Roo, Mexico. *Geological Society of America Special Papers, 404*, 105-128.

Strayer, D. L., May, S. E., Nielsen, P., Wollheim, W., & Hausam, S. (1997). Oxygen, organic matter, and sediment granulometry as controls on hyporheic animal communities. *Archiv fur Hydrobiologie (140)*, 131-144.

Taylor, M. P., Drysdale, R. N., & Karthew, K. D. (2004). The formation and environmental significance of calcite rafts in tropical tufa-depositing rivers of northern Australia. *Sedimentology*, 1081-1101.

Taylor, P. M., & Chafetz, H. S. (2004). Floating rafts of calcite crystals in cave pools, central Texas, U.S.A.: crystal habit vs. saturation state. *Journal of Sedimentary Research*.

Teng, H. H., Dove, P. M., & De Yorea, J. J. (2000). Kinetics of calcite growth: Surface processes and relationships to macroscopic rate laws. *Geochimica et Cosmochimica Acta, Vol. 64, No. 13*, 2255-2266.

van Hengstum, P.J., Donnelly, J.P., Fall, P.L., Toomey, M.R., Albury, N.A., Kakuk, B., 2016b. The intertropical convergence zone modulates intense hurricane strikes on the western North Atlantic margin. Scientific Reports 6, 21728.

White, W. (1997). Thermodynamic equilibrium, kinetics, activation barriers, and reaction mechanisms for chemical reactions in karst terrains. *Environmental Geology 30 (1/2)*.